Acta Pharmaceutica Sinica B 2022;12(5):2268–2279

Chinese Pharmaceutical Association
Institute of Materia Medica, Chinese Academy of Medical Sciences

Acta Pharmaceutica Sinica B

www.elsevier.com/locate/apsb
www.sciencedirect.com

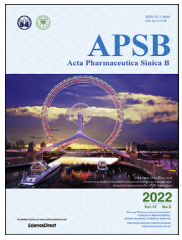

ORIGINAL ARTICLE

Anticarin-β shows a promising anti-osteosarcoma effect by specifically inhibiting CCT4 to impair proteostasis

Gan Wang[a,†], Min Zhang[a,b,†], Ping Meng[a,†], Chengbo Long[a,b,†], Xiaodong Luo[c,†], Xingwei Yang[c], Yunfei Wang[a,d], Zhiye Zhang[a], James Mwangi[a,b,e], Peter Muiruri Kamau[a,b,e], Zhi Dai[c], Zunfu Ke[f], Yi Zhang[g], Wenlin Chen[h], Xudong Zhao[a], Fei Ge[i], Qiumin Lv[a,e], Mingqiang Rong[a,e], Dongsheng Li[a], Yang Jin[j,*], Xia Sheng[k,*], Ren Lai[a,d,e,l,*]

[a]*Key Laboratory of Animal Models and Human Disease Mechanisms, Chinese Academy of Sciences/Key Laboratory of Bioactive Peptides of Yunnan Province, KIZ-CUHK Joint Laboratory of Bioresources and Molecular Research in Common Diseases, National Resource Center for Non-Human Primates, Kunming Primate Research Center, and National Research Facility for Phenotypic & Genetic Analysis of Model Animals (Primate Facility), Kunming Institute of Zoology, Kunming 650107, China*
[b]*University of Chinese Academy of Sciences, Beijing 100049, China*
[c]*State Key Laboratory of Phytochemistry and Plant Resources in West China, Kunming Institute of Botany, Chinese Academy of Sciences, Kunming 650201, China*
[d]*Institutes for Drug Discovery and Development, Chinese Academy of Sciences, Shanghai 201203, China*
[e]*Sino-African Joint Research Center, Chinese Academy of Science, Wuhan 430074, China*
[f]*Department of Pathology, First Affiliated Hospital, Sun Yat-sen University, Guangzhou 510080, China*
[g]*Department of Orthopaedic Surgery, First Affiliated Hospital of Zhengzhou University, Zhengzhou 450052, China*
[h]*Department of Breast Surgery, Third Affiliated Hospital of Kunming Medical University, Yunnan Cancer Center, Kunming 650118, China*
[i]*Department of Breast Surgery, First Affiliated Hospital of Kunming Medical University, Kunming 650032, China*
[j]*Department of Biosciences, University of Oslo, Oslo 0316, Norway*
[k]*Key Laboratory of Environment and Health, Ministry of Education & Ministry of Environmental Protection, And State Key Laboratory of Environmental Health, School of Public Health, Tongji Medical College, Huazhong University of Science and Technology, Wuhan 434000, China*
[l]*Center for Biosafety Mega-Science, Chinese Academy of Sciences, Wuhan 430071, China*

Received 16 September 2021; received in revised form 4 November 2021; accepted 30 November 2021

*Corresponding authors.
E-mail addresses: rlai@mail.kiz.ac.cn (Ren Lai), xiasheng@hust.edu.cn (Xia Sheng), yangj@ulrik.uio.no (Yang Jin).
[†]These authors made equal contributions to this work.
Peer review under responsibility of Chinese Pharmaceutical Association and Institute of Materia Medica, Chinese Academy of Medical Sciences.

https://doi.org/10.1016/j.apsb.2021.12.024

KEY WORDS

Proteostasis;
CCT;
TRiC;
Osteosarcoma;
STAT3;
Anticarin-β;
PDX model

Abstract Unlike healthy, non-transformed cells, the proteostasis network of cancer cells is taxed to produce proteins involved in tumor development. Cancer cells have a higher dependency on molecular chaperones to maintain proteostasis. The chaperonin T-complex protein ring complex (TRiC) contains eight paralogous subunits (CCT1-8), and assists the folding of as many as 10% of cytosolic proteome. TRiC is essential for the progression of some cancers, but the roles of TRiC subunits in osteosarcoma remain to be explored. Here, we show that CCT4/TRiC is significantly correlated in human osteosarcoma, and plays a critical role in osteosarcoma cell survival. We identify a compound anticarin-β that can specifically bind to and inhibit CCT4. Anticarin-β shows higher selectivity in cancer cells than in normal cells. Mechanistically, anticarin-β potently impedes CCT4-mediated STAT3 maturation. Anticarin-β displays remarkable antitumor efficacy in orthotopic and patient-derived xenograft models of osteosarcoma. Collectively, our data uncover a key role of CCT4 in osteosarcoma, and propose a promising treatment strategy for osteosarcoma by disrupting CCT4 and proteostasis.

1. Introduction

Osteosarcoma (OS) is a primary bone malignancy that mainly affects children and adolescents[1−3]. Approximately 85% of OS patients have metastasis, and their 5-year survival rate is less than 20%[4]. The mainstay of curative treatment for OS is surgical resection in combination with chemotherapy using drugs such as doxorubicin, cisplatin, and methotrexate, which are effective in patients with localized disease[5]. However, for patients with metastatic or relapsed OS, clinical outcome has barely improved during the past 30 years because of a lack of effective therapeutics[6]. Of the molecular alterations, activation of the receptor tyrosine kinases (RTKs), such as signal transducer and activator of transcription 3 (STAT3) signaling, is frequently observed in OS tumors[7].

Mounting evidence has suggested that cancer cells are highly dependent on the homeostasis of protein synthesis and degradation, also termed proteostasis[8]. T-complex protein ring complex (TRiC) belongs to type II chaperonin subfamily and is a cylindrically structured protein with two back-to-back rings, each of which is composed of eight paralogous subunits (CCT1−CCT8)[9]. Adenosine triphosphate binding and hydrolysis drive conformational change of TRiC to encapsulate and fold substrate polypeptides[10]. TRiC facilitates the folding of 10% of the cytosolic proteome, including many key structural and regulatory proteins, such as β-actin, tubulin[11], cell cycle regulator CDC20[12], VHL tumor suppressor[9], the TORC1 complex[13], and STAT3[14]. TRiC level is significantly elevated in multiple cancers and is associated with several essential biological processes in cancer progression[15−17]. Genetic inhibition of TRiC represses cancer cell growth[18], providing the rationale that TRiC may be a promising therapeutic target. TRiC subunit has a unique ability to assist the folding of select proteins[19]. However, the functional roles of TRiC in tumors have been poorly defined due to the paucity of specific inhibitors.

In this study, we show that CCT4/TRiC activity is tightly correlated and elevated in human OS. We identified a small molecule natural coumarin compound derived from the bark of the traditional Chinese medicine (*Antiaris toxicaria* Lesch.), anticarin-β, as a potent inhibitor of CCT4/TRiC. Anticarin-β shows remarkable antitumor efficacy in different orthotopic and patient-derived xenograft (PDX) models of OS by impeding CCT4-mediated maturation of STAT3. Therefore, our data implicate an important oncogenic role of CCT4/TRiC in OS and highlight the potential of targeting CCT4 as a novel treatment option for OS.

2. Materials and methods

2.1. Ethical statement and tissue collection

Paraffin-fixed tissue sections of human osteosarcoma (OS) specimens were collected at the First Affiliated Hospital of Sun Yat-sen University (Guangzhou, China). Frozen tissues of human OS specimens were collected at the First Affiliated Hospital of Zhengzhou University (Zhengzhou, China). The samples were obtained upon informed consent from patients and was ethically approved by the Ethics Committee of both hospitals.

2.2. Antibodies

Primary antibodies against caspase-3 (9665, CST), caspase-7 (ab32522, Abcam), CCT4 (ab205013, Abcam), GAPDH (97166, CST), PARP (9532, CST), p-STAT1 (Tyr701) (7649, CST), p-STAT2 (Tyr690) (4441, CST), p-STAT3 (Ser727) (9134, CST), p-STAT3 (Tyr705) (9145, CST), p-STAT5 (Tyr694) (4322, CST), p-STAT6 (Tyr641) (9361, CST), STAT1 (9172, CST), STAT3 (12640, CST), STAT5 (94205, CST), STAT6 (5397, CST), XIAP (2045, CST), LC3 (12741, CST), β-catenin (8480, CST), N-cadherin (13116, CST), β-actin (3700, CST), and secondary goat anti-mouse HRP-IgG (7076, CST) and goat anti-rabbit HRP-IgG (7074, CST) antibodies were used for immunoblotting. Primary antibodies against KI67 (9449, CST), CD3 (ab135372, Abcam), CD68 (76437, CST), CD56 (99746, CST), and secondary Fluorescein AffiniPure goat anti-rabbit IgG (111-095-144, Jackson) and Cy3 AffiniPure goat anti-rabbit IgG (111-165-144, Jackson) antibodies were used for immunofluorescence. Antibodies against p-STAT3 (Tyr705) (9145, CST), STAT3 (9139, CST), cleaved caspase-3 (Asp175) (9661, CST), and CCT4 (ab129072, Abcam) were used for immunohistochemistry.

2.3. Cell culture

The human cell lines EJ-1 (CRL-3380, ATCC), HCT 116 (CCL-247, ATCC), MCF7 (HTB-22, ATCC), MDA-MB-231 (HTB-26, ATCC), NCI-H157 (CRL-5802, ATCC), NCI-H292 (CRL-1848, ATCC), NCI-H460 (HTB-177, ATCC), NCI-H661 (HTB-183, ATCC), and T24 (HTB-4, ATCC) were cultured in RPMI-1640 medium (Cellgro, Corning). Human 801-D (200690YJ, KCB, Kunming, China), HEK-293T (CRL-11268, ATCC), HeLa (CCL-2, ATCC), HLF-a (CCL-199, ATCC), HT-29 (HTB-38, ATCC), HUVEC (PCS-100-013, ATCC), LX-2 (337957, BNCC, Beijing, China), SK-MES-1 (HTB-58, ATCC), T98G (CRL-1690, ATCC), and U-87 MG (HTB-14, ATCC) cells were maintained in Dulbecco's modified Eagle medium (DMEM, Cellgro). Human A549 (CCL-185, ATCC), HepG2 (HB-8065, ATCC), K-562 (CCL-243, ATCC), MG-63 (CRL-1427, ATCC), PANC-1 (CRL-1469, ATCC), SaOS2 (HTB-85, ATCC), U2OS (HTB-96, ATCC), and NSC cells were maintained in DMEM: Nutrient Mixture F-12 (Cellgro). The cell lines GBM-18 and GBM-3 were cultured in DMEM (Cellgro).

All culture media was supplemented with 10% fetal bovine serum, 100 unit/mL penicillin and 100 unit/mL streptomycin, and were maintained in a humidified atmosphere containing 5% CO_2 in an incubator at 37 °C.

2.4. Quantification and statistical analysis

Statistical analysis was conducted with GraphPad Prism 6.0 (GraphPad Software). When needed, a d'Agostino-Pearson normality test was performed and was followed by Student's *t*-tests or non-parametric Mann−Whitney tests when the distribution was not normal. Statistical comparisons between groups were conducted with ordinary one-way analysis of variance with multiple comparisons tests. All results are presented as the

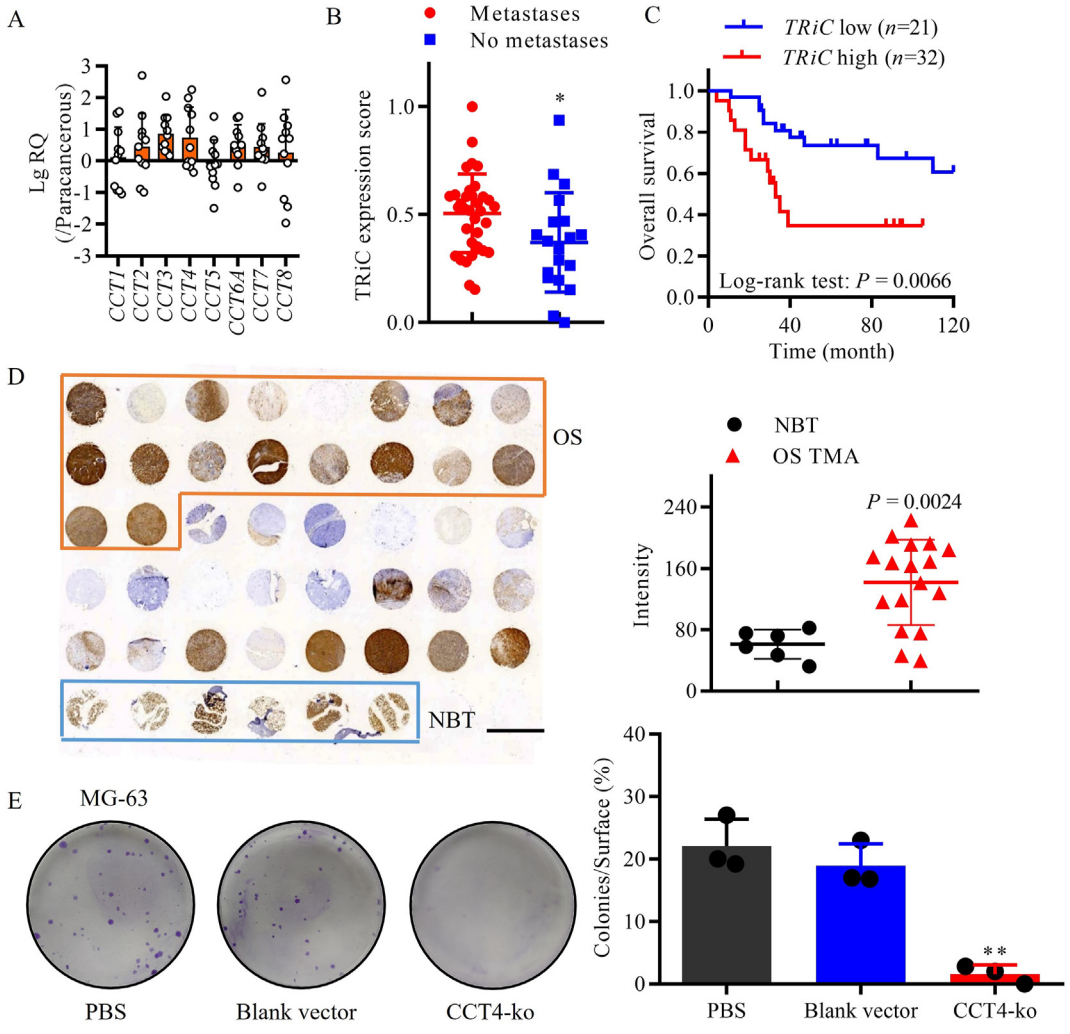

Figure 1 The expression of TRiC subunits is increased in human osteosarcoma (OS). (A) Quantitative reverse transcription PCR analysis of the expression of TRiC subunits in OS tissues and matched para-cancerous bone tissues ($n = 11$). Relative quantification (RQ) for each subunit is presented as a dot-box plot. (B) TRiC expression was compared in patients with or without metastasis in the GSE21257 dataset. (C) Association between TRiC activity score and overall survival of the patients was estimated by Kaplan−Meier analysis. (D) Immunohistochemical analysis of CCT4 in OS tissues (17 cases in TMA (Tissue microarray)) and NBT (normal bone tissue, $n = 6$). Scale bar, 2 mm. (E) CCT4 knockout MG-63 cells were generated, and then the cells were plated and cultured for colony formation assays. The data are presented as the mean ± SD, $n = 3$. *$P < 0.05$; **$P < 0.01$, two-tailed *t*-test.

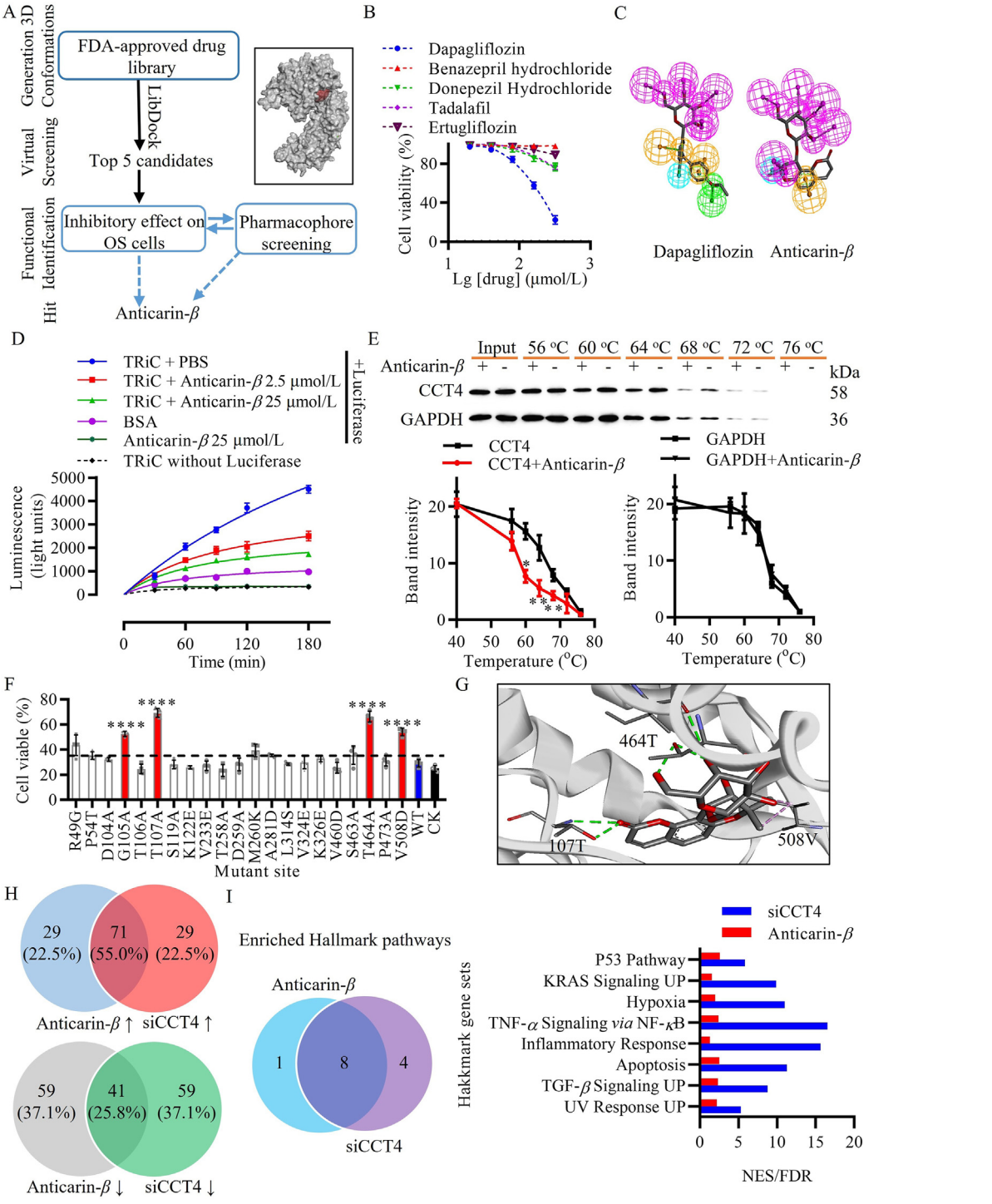

Figure 2 Anticarin-β inhibits the chaperonin activity of TRiC through interaction with CCT4. (A) Workflow for identification of CCT4 binding compounds, which mainly consists of virtual screening, pharmacophore screening, and experimental validation. The box represented the 3D structural of CCT4 and binding site (red boll) for virtual screening. (B) The viability of MG-63 cells treated with the top 5 candidates on the screen. Dapagliflozin IC_{50} ~200 μmol/L, $n = 3$. (C) Comparison of the 3D pharmacophores of anticarin-β and dapagliflozin, purple/green spheres represent electron acceptor/donor, yellow spheres represent ring aromatic, blue spheres represent hydrophobe group. (D) The luciferase refolding assay was performed to measure the inhibitory effect of anticarin-β on the chaperonin activity of purified human TRiC. Bovine albumin was used as a negative control. The mean ± SD from three representative experiments is shown. (E) The cellular thermal shift assay was performed on intact MG-63 cells with 2.5 μmol/L anticarin-β. The band intensity values were calculated from three independent experiments. The points and error bars represent the mean ± SD, $n = 3$; $^{*}P < 0.05$, $^{**}P < 0.01$ *versus* the control group, two-tailed *t*-test. (F) CCT4 mutant plasmids were transfected into U2OS cells followed by 1 μmol/L anticarin-β treatment for 20 h. Cell viability was analyzed by trypan blue. The points and error bars represent the mean ± SD, $n = 4$; $^{****}P < 0.0001$ *versus* the WT group, two-tailed *t*-test. CK, blank vector; WT, wild type CCT4. (G) 3D structure of the binding site of anticarin-β with CCT4, the green dotted lines represent hydrogen bonds, and the pink dotted lines represent alkyl hydrophobic bonds. (H) Venn diagrams show the number of overlapped genes among top 100 significantly up-regulated (↑) and down-regulated (↓) genes in OS cells with anticarin-β or siCCT4 treatment. (I) Hallmark GSEA shows a significant overlap of enriched pathways in OS cells between anticarin-β and siCCT4 treatment. Bar plot shows commonly enriched Hallmark pathways with FDR < 0.25. The numbers represent the normalized enrichment scores (NES) for the corresponding gene sets.

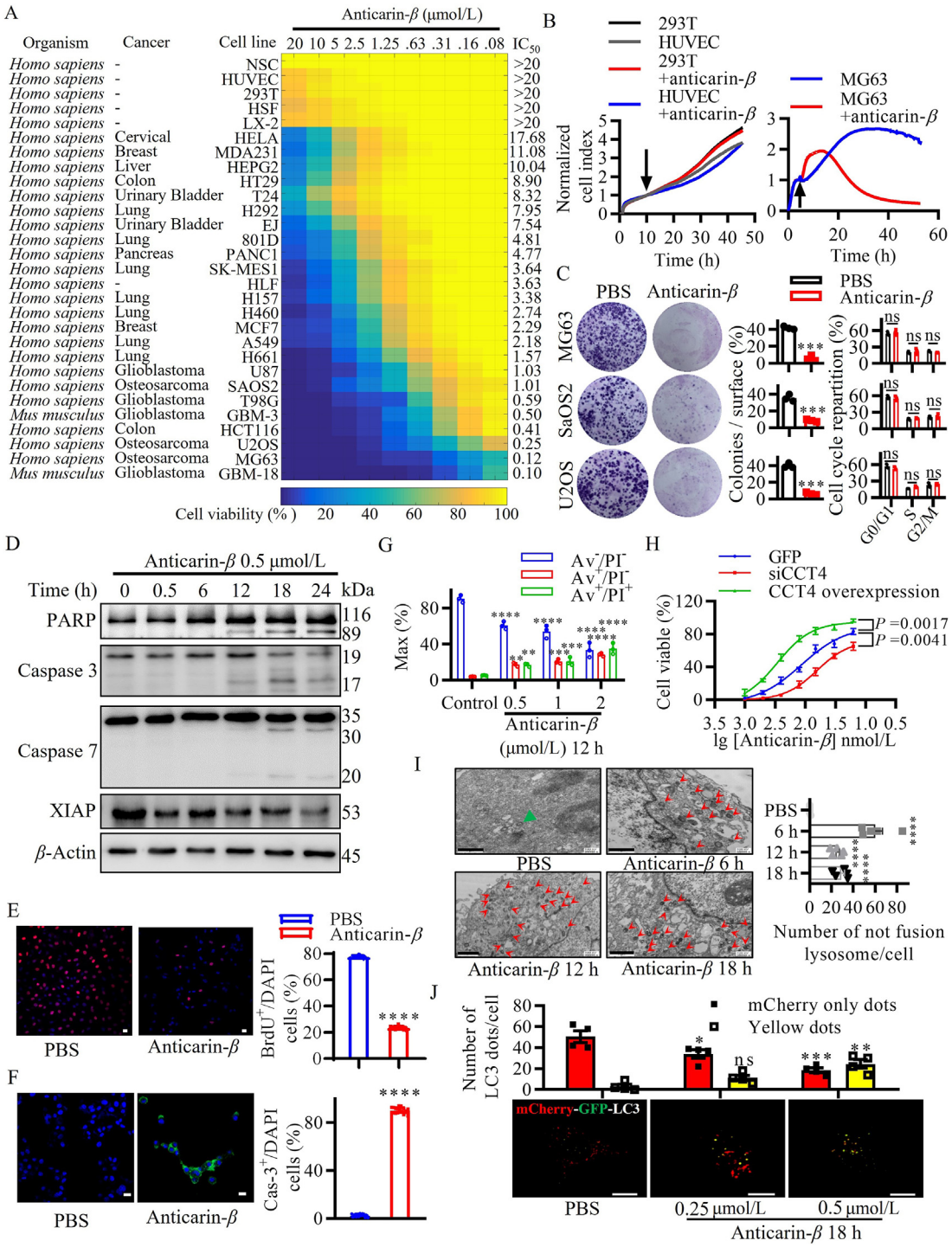

Figure 3 Anticarin-β inhibits OS cell growth by inducing apoptosis and disrupting autophagosome degradation. (A) Heatmap showing the selective cytotoxicity of anticarin-β towards a panel of normal and cancer cell lines. The cells were treated with a serial concentration of anticarin-β for 48 h. Cell viability was measured by MTT assay, and the IC_{50} was determined, $n = 4$. (B) The real-time cell analysis data show that anticarin-β has selective cytotoxicity on osteosarcoma cells (left, anticarin-β 0.5 μmol/L) compared with non-malignant cells (right, anticarin-β 2 μmol/L). Arrows indicate the time that anticarin-β was applied. (C) OS cells were treated with 0.05 μmol/L anticarin-β for 1 day and then plated for colony formation. Anticarin-β has no effects on the cell cycle distribution of OS cells. OS cells were treated with 0.5 μmol/L anticarin-β for 12 h, and the proportion of cells in G0/G1, S, G2/M, was determined by PI (propidium iodide) staining. The points and error bars represent the mean ± SD, $n = 3$; ns, not significant; ***$P < 0.001$ *versus* the phosphate buffered saline (PBS) group, two-tailed *t*-test. (D) MG-63 cells were treated with 0.5 μmol/L anticarin-β for the indicated durations before being analyzed by Western blot. (E) BrdU analysis of MG-63 cells treated with either PBS or anticarin-β. Scale bar, 20 μm. The data represent mean ± SD, $n = 20$; ****$P < 0.0001$ *versus* the PBS group, two-tailed *t*-test. (F) MG-63 cells were loaded with caspase 3/7 green probes and then treated with 0.5 μmol/L anticarin-β or vehicle for 24 h. An increase in fluorescence indicated the occurrence of apoptosis. Scale bar, 1 μm. The data represent mean ± SD, $n = 20$; ****$P < 0.0001$ *versus* the PBS group, two-tailed *t*-test. (G) After treatment with

means ± standard deviation (SD) or standard error of mean (SEM) from at least three independent measurements. The P values were calculated, and significance is represented as follows: $^{*}P < 0.05$, $^{**}P < 0.01$, $^{***}P < 0.001$), and $^{****}P < 0.0001$.

Additional methods and references are available at Supporting Information.

3. Results

3.1. TRiC signaling is activated in OS and correlates with poor outcome

We first investigated the possible involvement of TRiC signaling in OS by interrogating the publicly available gene expression datasets of OS. The interrogation of the PREdiction of Clinical Outcomes from Genomic Profiles (PRECOG) database showed that gene expression of chaperonins was significantly associated with prognosis in various cancers, particularly in OS (Supporting Information Table S1A). Of note, TRiC showed the highest PRECOG score in OS amongst the chaperonin subfamily (Tables S1B and S1C). The expression of all TRiC subunits was significantly increased in the OS tissues compared to in the paired normal bone tissues (Fig. 1A). To further assess whether TRiC level is associated with OS development, we analyzed the correlation of TRiC expression with metastatic status and overall survival. The expression of TRiC subunits was significantly higher in patients with metastasis and the overall expression of TRiC subunits poor overall survival (Fig. 1B and C and Supporting Information Fig. S1A, see Supporting Information Table S2 for primers information). Together, these results indicate that the activity of TRiC signaling is correlated with OS progression and prognosis.

Next, we evaluated the *in vitro* efficacy of TRiC subunits in OS cell lines. Colony formation analysis revealed that knockdown of CCT4 or CCT7 significantly reduced the clonogenicity of MG-63 cells (Fig. S1B, see Supporting Information Table S3 for detailed siRNA information). This is in line with a recent structure study demonstrating that the CCT4 subunit plays a key role in mediating the function of TRiC[19–21]. Hereafter, we focused on CCT4 as a surrogate of TRiC in the following characterization. Consistent with the above observation, immunohistochemical analysis revealed significantly elevated level of CCT4 in OS compared to in normal tissues (Fig. 1D, see Supporting Information Table S4 for detailed group information). Interestingly, CCT4 knockout using CRISPR/Cas9 approach was lethal to OS cells, with no viable clone obtained after 2 weeks (Fig. 1E). Alternatively, we performed subsequent functional analyses by CCT4 knockdown, which significantly affected the migration and invasion of MG-63 cells, but showed little effect on apoptosis, autophagy, and proliferation (Supporting Information Fig. S2). These results corroborated an indispensable role of CCT4/TRiC in OS cell survival and proposed CCT4 as a potential therapeutic target for OS.

3.2. Discovery of anticarin-β as an inhibitor of the CCT4 subunit of TRiC

Despite these findings, the paucity of available inhibitors impeded us from further evaluation. To overcome this barrier, we first performed a model-based virtual screen of the United States Food and Drug Administration-approved drug library, intending to search for potential inhibitors for the CCT4 subunit of TRiC (Fig. 2A). This gave rise to several compounds that potentially bind CCT4 (Supporting Information Table S5). Then, we evaluated the effect of the top 5 compounds on the growth of MG-63 cells, in which the CCT4 level is slightly lower compared to in U2OS and SaOS2 cells (Fig. S2B). We found that dapagliflozin, a drug for type 2 diabetes, showed the strongest inhibitory activity relative to the other candidates, with a half-maximal inhibitory concentration (IC_{50}) of 200 μmol/L (Fig. 2B). To search for more potent inhibitors, we created a three-dimensional pharmacophore model of dapagliflozin (Fig. 2C) and screened an in-house chemical library. A natural compound anticarin-β (#1993560, the Cambridge Crystallographic Data Centre) with a 3D pharmacophore highly similar to that of dapagliflozin was identified (Fig. 2C).

To verify the inhibitory effect of anticarin-β, a luciferase refolding assay was performed with purified TRiC, whose activity remains *in vitro*[22]. Anticarin-β dose-dependently inhibited the refolding of denatured luciferase by isolated TRiC (Fig. 2D). Furthermore, the surface plasmon resonance-based binding assay showed that anticarin-β bound to immobilized recombinant CCT4 protein with an affinity (K_D ~2.2 μmol/L) significantly higher compared to with other TRiC subunits (Supporting Information Fig. S3A), indicating a direct and specific interaction of anticarin-β with CCT4. To assess whether anticarin-β also binds to CCT4 *in vivo*, we performed the cellular thermal shift assay, an approach to determine the effect of ligand binding on the thermal stability of target proteins in live cells[23]. Compared with control, anticarin-β treatment resulted in significantly lower thermal stability of CCT4 in MG-63 cells at denaturation temperature from 60 to 68 °C (Fig. 2E). GAPDH was used as a control and exhibited no difference in thermal stability upon anticarin-β treatment, indicating a specific ligand effect on CCT4.

3.3. Anticarin-β inhibits TRiC activity by specifically binding to its CCT4

Subsequently, we mapped the binding site of anticarin-β in CCT4 using both *in silico* and experimental approaches. Blind docking experiment identified 4 potential binding pockets for anticarin-β in the protein structure of CCT4. Next, a 100 ns molecular dynamics simulation was performed to determine the contribution of specific amino acid residues to the stability of anticarin-β binding (Supporting Information Fig. S3B and Table S6). Mutagenesis analysis revealed that four residues (G105, T107, T464, and

various concentrations of anticarin-β for 12 h, the apoptotic cells were stained by Annexin V and PI staining. The cells at the stage of early apoptosis (Av^+/PI^-) or late apoptosis (Av^+/PI^+) were quantified by flow cytometry. The data represent mean ± SD, $n = 3$; $^{***}P < 0.001$, $^{****}P < 0.0001$ *versus* the control group, two-tailed t-test. (H) Ectopic expression of CCT4 protected, whereas siRNA-mediated knockdown of CCT4 promoted, cell death of MG-63 induced by anticarin-β (two-tailed t-test, $n = 3$). (I) Electron microscopy images showing the autophagosomes (green arrow) and lysosomes (red arrow) in MG-63 cells treated with PBS or 0.5 μmol/L anticarin-β for the indicated times. Scale bar, 1 μm. The data represent mean ± SD, $n = 5$; $^{****}P < 0.0001$ *versus* the PBS group, two-tailed t-test. (J) MG-63 cells expressing mCherry-GFP-LC3 were treated with 0.25 and 0.5 μmol/L anticarin-β for 24 h. Autophagosomes (yellow) and autolysosomes (red) were counted. Scale bar, 20 μm. Data are mean ± SD; $^{***}P < 0.001$, $^{**}P < 0.01$, $^{*}P < 0.05$; ns, not significant; two-tailed t-test, compared with the PBS group.

V508) at site 2 may be critical for anticarin-β binding. This was confirmed by cell viability assay where mutation of these residues in CCT4 significantly prevented the cytotoxicity of anticarin-β in U2OS cells (Fig. 2F and G, see Supporting Information Table S7 for primers information of point mutation). Isothermal titration calorimetry was used to study binding affinity constants of anticarin-β with different point mutants of CCT4. The affinity (K_D) between the CCT4 mutants and anticarin-β decreased by 3−26 times compared to the wild-type CCT4 (Supporting Information Fig. S4). 3D structure modeling further suggested that these three mutant residues (T107, T464, and V508) may interact directly with anticarin-β (Fig. 2G). Importantly, transcriptomic analysis revealed that the effect of anticarin-β on global gene expression was highly concordant to that of CCT4 depletion (Fig. S3C). Amongst the top 100 up-regulated genes, there were 71 commonly occurred in both treatments, whereas 41 in the top 100 down-regulated (Fig. 2H). This led to the enrichment of similar oncogenic pathways, such as Hallmark P53 pathway, KRAS signaling, hypoxia, and apoptosis (Fig. 2I). Together, these data demonstrate that anticarin-β inhibits TRiC activity by specifically binding to its CCT4 subunit.

3.4. *Anticarin-β inhibits survival and induces apoptosis in OS cells*

To assess the potential cytotoxicity of anticarin-β, we explored the effect of anticarin-β on the viability of a series of non-cancerous and cancer cell lines. Interestingly, dose-dependent inhibition of viability was observed for all cancer cell lines tested, whereas no significant cytotoxic effect was detected on the non-malignant cell lines (Fig. 3A). Notably, the OS and glioblastoma cell lines were more sensitive to anticarin-β than the other cancer cell lines (Fig. 3A). In a time−course assay, 0.5 μmol/L anticarin-β decreased the viability of MG-63 cells by ∼73% within 24 h, whereas no toxicity was observed in HEK-293T and HUVEC cells (Fig. 3B). Concerning the long-term cell growth, colony-forming assay revealed that anticarin-β inhibited the growth of three OS cell lines, MG-63, U2OS, and SaOS2, by approximately 95% (Fig. 3C). Cell cycle distribution was not significantly altered in response to anticarin-β (Fig. 3C), indicating that anticarin-β may not arrest cell cycle or suppress proliferation in OS cells. These data suggest that anticarin-β effectively inhibits the viability and growth of OS cells *in vitro*.

Another possible explanation to these findings is that anticarin-β likely induces cell death rather than cell cycle arrest in OS cells. To test this, we examined apoptotic markers by Western analysis in MG-63 cells treated with anticarin-β. There was a sharp increase in the level of cleaved PARP and cleaved caspase-3/7 after 12 h of anticarin-β treatment, which was accompanied by a rapid decline in the expression of XIAP (Fig. 3D). Compared with the control treatment (PBS), anticarin-β treatment significantly inhibits cell proliferation (Fig. 3E), as demonstrated by BrdU staining. Utilizing the CellEvent caspase-3/7 Green probe, we verified that caspase-3/7 cleavage was induced in approximately 80% of MG-63 cells treated with anticarin-β, whereas the ratio was lower than 5% in the control cells (Fig. 3F). Consistently, Annexin V-FITC assay and propidium iodide fluorescence staining also showed significantly stronger signals in cells exposed to anticarin-β relative to control (Fig. 3G). Importantly, ectopic expression of CCT4 partially rescued MG-63 cells from apoptosis induced by anticarin-β (Fig. 3H). These results indicate that anticarin-β exerts antitumor effect by inducing apoptosis in OS cells.

Since TRiC depletion was recently shown to confer impaired autophagy and sensitivity to apoptotic insults[24], we further determined whether blocked autophagic flux mediates the anticarin-β-induced apoptosis. Transmission electron microscopic analysis of MG-63 cells treated with anticarin-β revealed a dramatic increase in the number of autophagosomes, which did not appear to merge with lysosomes (Fig. 3I). To investigate whether autophagosome-lysosome fusion was hindered, we transfected MG-63 cells with the tandem-labeled mCherry-Green fluorescent protein (GFP)-LC3 construct to distinguish autophagosomes and autolysosomes[25]. Indeed, anticarin-β treatment significantly increased the number of autophagosomes and decreased the number of autolysosomes (Fig. 3J). These data implicate that anticarin-β blocks autophagosome−lysosome fusion and impairs autophagy, which may mediate cell death.

3.5. *Anticarin-β inhibits TRiC-mediated STAT3 maturation and activation*

To uncover the genes or pathways that may contribute to the differential sensitivity to anticarin-β, we analyzed the correlation between the IC_{50} of the tested cell lines and their gene expression profiles using the Cancer Cell Line Encyclopedia[26]. The expression of CLEC11A, a member of the C-type lectin superfamily encoding the stem cell growth factor, showed the most significant correlation with anticarin-β sensitivity (Fig. 4A). Despite the limited knowledge about its role in cancer, further interrogation of the PharmacoDB database[27] showed that CLEC11A expression in cancer cells strongly predicted sensitivity to inhibitors of the RTKs, especially type III RTKs (Fig. 4A). These bioinformatic analyses establish a link between anticarin-β activity and RTKs signaling.

To gain a better insight into this connection in the context of OS, we performed a phospho-kinase antibody array of RTK pathways in MG-63 cells treated with anticarin-β. Interestingly, anticarin-β significantly reduced the levels of phosphorylated (p-) STAT proteins, while it induced AKT and ERK activation (Fig. 4B). Western blot validated that both p- and total STAT3 level was robustly attenuated in MG-63 cells in response to anticarin-β (Fig. 4C), a phenotype that can be rescued by CCT4 overexpression (Fig. 4D). Similar to CCT4 knockdown, anticarin-β significantly reversed the expression of a series of genes directly regulated by STAT3 in the RNA-seq analysis (Fig. 4E), in particular the level of pro-apoptotic genes (Fig. 4F)[28]. These data suggest that the apoptosis-inducing effect of anticarin-β may be mediated, at least in part, by repressing STAT3 signaling.

A recent study evidenced that TRiC is critical for the proper folding and activation of STAT3[14]. To evaluate whether anticarin-β inhibits this process, we generated MG-63 cells expressing GFP (control), wild-type STAT3 (STAT3-WT), dominant-negative STAT3 (STAT3-DN), or constitutively active STAT3 (STAT3-CA) *via* lentivirus transduction (Fig. 4G). As expected, compared with GFP control, STAT3-WT and STAT3-DN did not protect the cells from apoptosis induced by anticarin-β. Interestingly, introduction of STAT3-CA only slightly rescued the apoptotic phenotype (Fig. 4G), suggesting that anticarin-β may disrupt the TRiC-mediated folding and maturation of STAT3, including its constitutively active variant.

3.6. *Anticarin-β inhibits tumor growth in an orthotopic mouse model of OS*

Building on the significant *in vitro* effect and the mechanism of action, we further evaluated the *in vivo* efficacy of anticarin-β in preclinical models of OS. To this end, we first determined the maximum tolerated dose of anticarin-β to define the optimal *in vivo* concentration. No lethality or apparent toxicity was

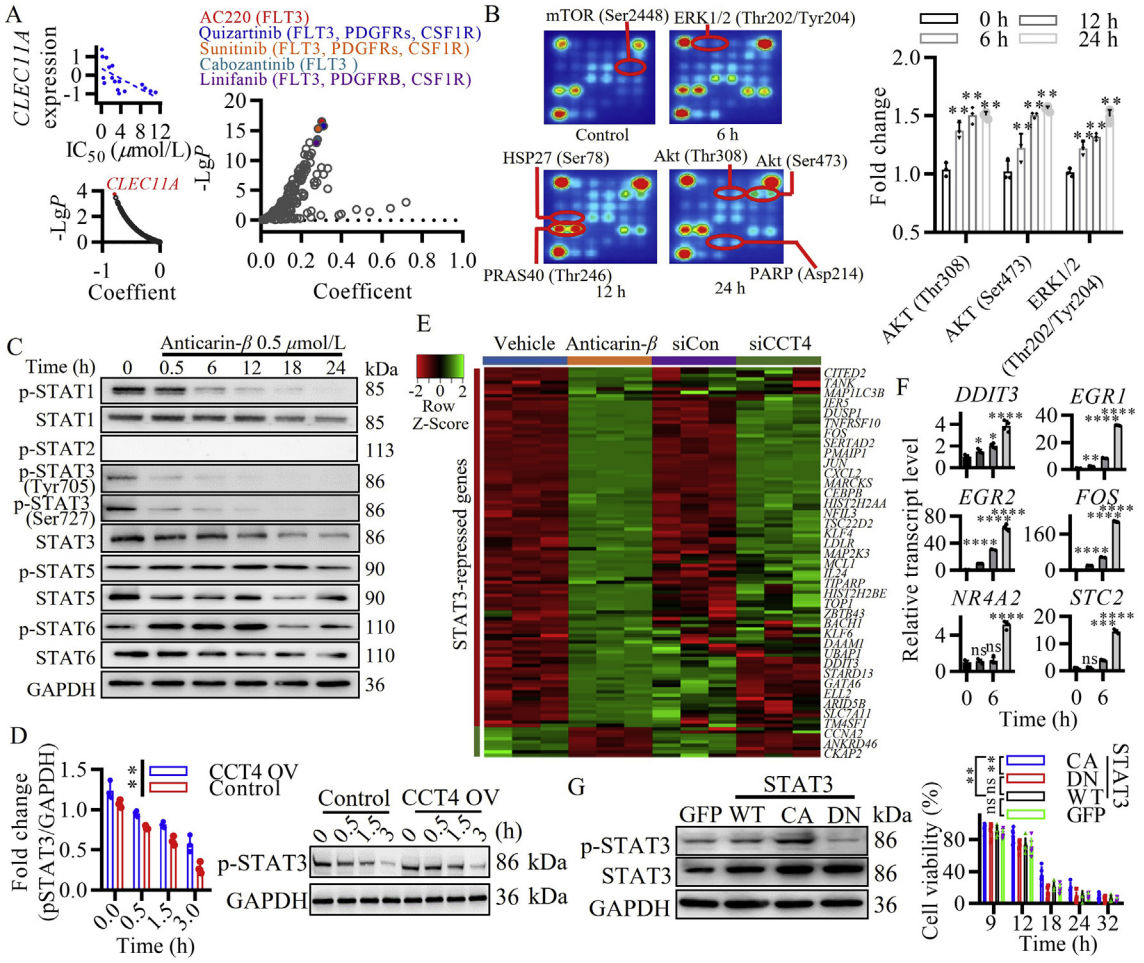

Figure 4 Anticarin-β inhibits STAT3 expression and activation. (A) Pearson correlation analysis of anticarin-β efficiency with CLEC11A expression in cancer cell lines. The coefficients (r-value) and P values were calculated for the correlations between genome-wide gene expression profiles and the IC_{50} of anticarin-β (in Fig. 3A) across all overlapping cell lines ($n = 24$). The correlation coefficients are shown on the x-axis, and the $-\log$ (P values) are shown on the y-axis. PharmacoDB was then used to query the correlation between the expression of CLEC11A and the sensitivities of cancer cell lines to various compounds. (B) Antibody array analysis of AKT and ERK1/2 activation upon anticarin-β treatment. The data are represented as mean ± SD, $n = 3$; $^{**}P < 0.01$ *versus* the control group, two-tailed t-test. (C) MG-63 cells were treated with anticarin-β and subjected to Western analysis for STATs. Anticarin-β inhibits STATs activation. MG-63 cells were exposed various hours to 0.5 μmol/L anticarin-β. Lysates were analyzed by Western blotting using the indicated antibodies. One representative experiment of three is shown. (D) Overexpression of CCT4 could delay the inactivation of p-STAT3 induced by anticarin-β in MG-63 cells. MG-63 cells were transfected with plasmids as indicated in the overexpression of CCT4 or GFP control plasmids. The levels of p-STAT3 were analyzed by Western blotting. One representative experiment of three is shown. The data are represented as mean ± SD, $n = 3$, $^{**}P < 0.01$ *versus* the control group, two-tailed t-test. (E) Heatmap showing the expression of STAT3-regulated genes in MG-63 cells upon either anticarin-β (1 μmol/L) treatment or CCT4 knockdown. siCon, siRNA control (GSE166143). (F) MG-63 cells were treated with anticarin-β and before subjected to quantitative reverse transcription PCR analysis of the expression of STAT3-repressed pro-apoptotic genes. The data are represented as mean ± SD, $n = 4$; ns, not significant; $^{*}P < 0.05$, $^{**}P < 0.01$, $^{***}P < 0.001$, $^{****}P < 0.0001$ *versus* the control group, two-tailed t-test. (G) MG-63 cells were introduced with the indicated form of STAT3 isoform, treated with anticarin-β, and cell viability was measured. STAT3 CA: constitutively active STAT3, A662C, and N664C; STAT3 DN: dominant-negative STAT3, Y705F; STAT3 WT: wild-type STAT3. The data are represented as mean ± SD, $n = 4$; ns, not significant; $^{**}P < 0.01$, two-tailed t-test.

observed within 50 days at doses up to 20 mg/kg (Fig. 5A). A pharmacokinetic study on anticarin-β in CD-1 mice showed that anticarin-β had comparable $t_{1/2}$ values in plasma and muscle (1.08−1.46 h), and could be almost eliminated within 8 h (Fig. 5B and Supporting Information Table S8). Therefore, daily administration of anticarin-β at a dose of 5 mg/kg was used for animal experiments.

Based on the favorable *in vitro* cytotoxicity and *in vivo* safety results, we first evaluated the efficacy of anticarin-β in an orthotopic xenograft model of OS, in which luciferase-expressing MG-63 cells were transplanted into BALB/c nude mice. The tumor-bearing mice were treated with or without anticarin-β (0.5 or 5 mg/kg/day) and tumor growth was monitored by measurement of bioluminescence. Two commonly used first-line therapeutic drugs for OS, methotrexate (20 mg/kg/twice a week) and cisplatin (5 mg/kg/day), were also included for comparison. Relative to vehicle treatment (control), anticarin-β treatment led to significant dose-dependent tumor regression, whereas methotrexate and cisplatin only slightly

inhibited tumor growth (Fig. 5C and D and Supporting Information Fig. S5A). About 40% of control tumor-bearing mice died within 49 days, suggesting successful transplantation of human MG-63 cells (Fig. 5E). In agreement with the effect on tumor growth, anticarin-β at both 0.5 and 5 mg/kg markedly improved the survival of tumor-bearing mice. In contrast, despite the moderate efficacy, cisplatin treatment did not improve the survival rate, whereas methotrexate treatment even worsened it (Fig. 5E). Following this, methotrexate treatment resulted in remarkable body weight loss of the mice, whereas anticarin-β (5 mg/kg) significantly prevented tumor-caused weight loss compared with the vehicle control (Fig. 5F), indicating no obvious toxicity and improved well-being of the mice. This was further confirmed by histological analysis of major organs, which showed no observable difference between the vehicle and 5 mg/kg anticarin-β treated groups (Fig. 5G).

Next, we examined the effect of anticarin-β on the activity of STAT3 signaling in the transplanted tumors. In line with the *in vitro* findings, STAT3 and p-STAT3 protein levels were both decreased in the tumor tissues of mice treated with anticarin-β, while cleaved caspase 3 was significantly induced (Fig. 5H, Fig. S5B and S5C). These results corroborate that anticarin-β effectively inhibits tumor growth and STAT3 activation *in vivo*.

3.7. *Anticarin-β inhibits tumor growth in multiple PDX models of OS*

To further evaluate the clinical utility of this compound, *ex vivo* 3D culture and mouse PDX models were generated. Three different PDX models derived from different stages of OS,

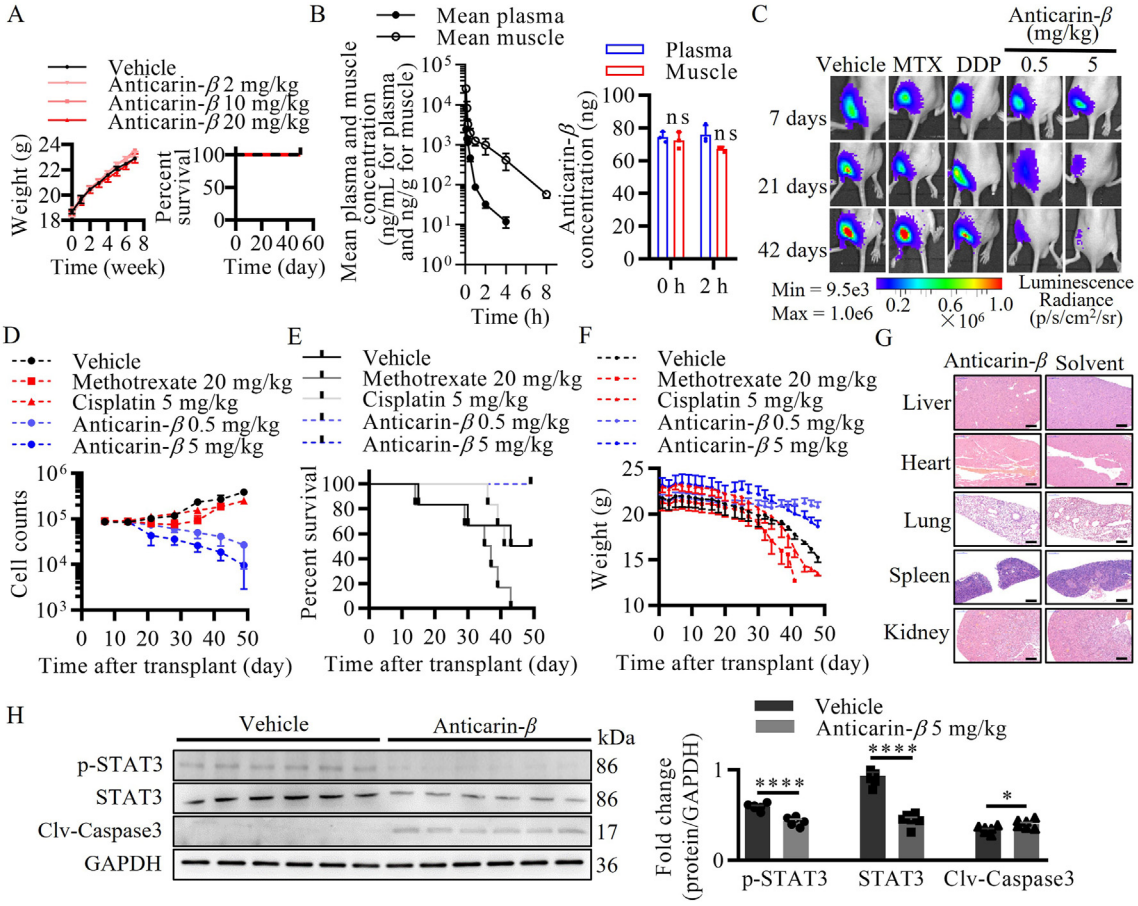

Figure 5 The anticancer effect of anticarin-β in an orthotopic model of OS. (A) Event-free survival curves and weight curves indicated that 20 mg/kg anticarin-β is safe for CD-1 mice. The data are presented as mean ± SD for 3 mice. (B) Mean plasma and muscle concentration profiles of anticarin-β in male CD-1 mice (n = 6) following a single i.m. injection of anticarin-β at 1 mg/kg. The findings suggest that anticarin-β is effectively distributed to the muscle. Anticarin-β concentrations in plasma and muscle were quantitated by liquid chromatography−tandem mass spectrometry. Anticarin-β in male CD-1 mouse plasma (EDTA-K2) and muscle homogenate was stable at room temperature for 2 h, n = 3. The data are represented as mean ± SD, ns, not significant, two-tailed t-test. (C−F) An orthotopic OS model was generated in BALB/c nude mice using MG-63-Luc cells. The mice were intramuscularly administered vehicle, methotrexate (20 mg/kg/twice a week), cisplatin (DDP, 5 mg/kg/day), or anticarin-β (0.5 or 5 mg/kg/day). Tumor growth was monitored by measurement of fluorescence weekly. The effects of the indicated treatments on tumor growth in tumor-bearing mice (C), the recorded tumor burden (D), survival (E), and body weight (F) are presented. The data are presented as mean ± SD, n = 6. (G) Anticarin-β (5 mg/kg) had no toxicity towards the main visceral organs. Representative hematoxylin−eosin staining of the main visceral organs (livers, kidneys, lungs, hearts, and spleens) of mice treated with 5 mg/kg/day anticarin-β or solvent (n = 6). Scale bar, 500 μm. (H) Tumors from mice treated with anticarin-β or vehicle were subjected to Western analysis, and the level of cleaved caspase3 (Clv-caspase3), p-STAT3, and STAT3 were evaluated. The intensity of each protein was quantified using ImageJ. The data are represented as mean ± SD, n = 6; $^*P < 0.05$, $^{****}P < 0.0001$ *versus* the vehicle group, two-tailed t-test.

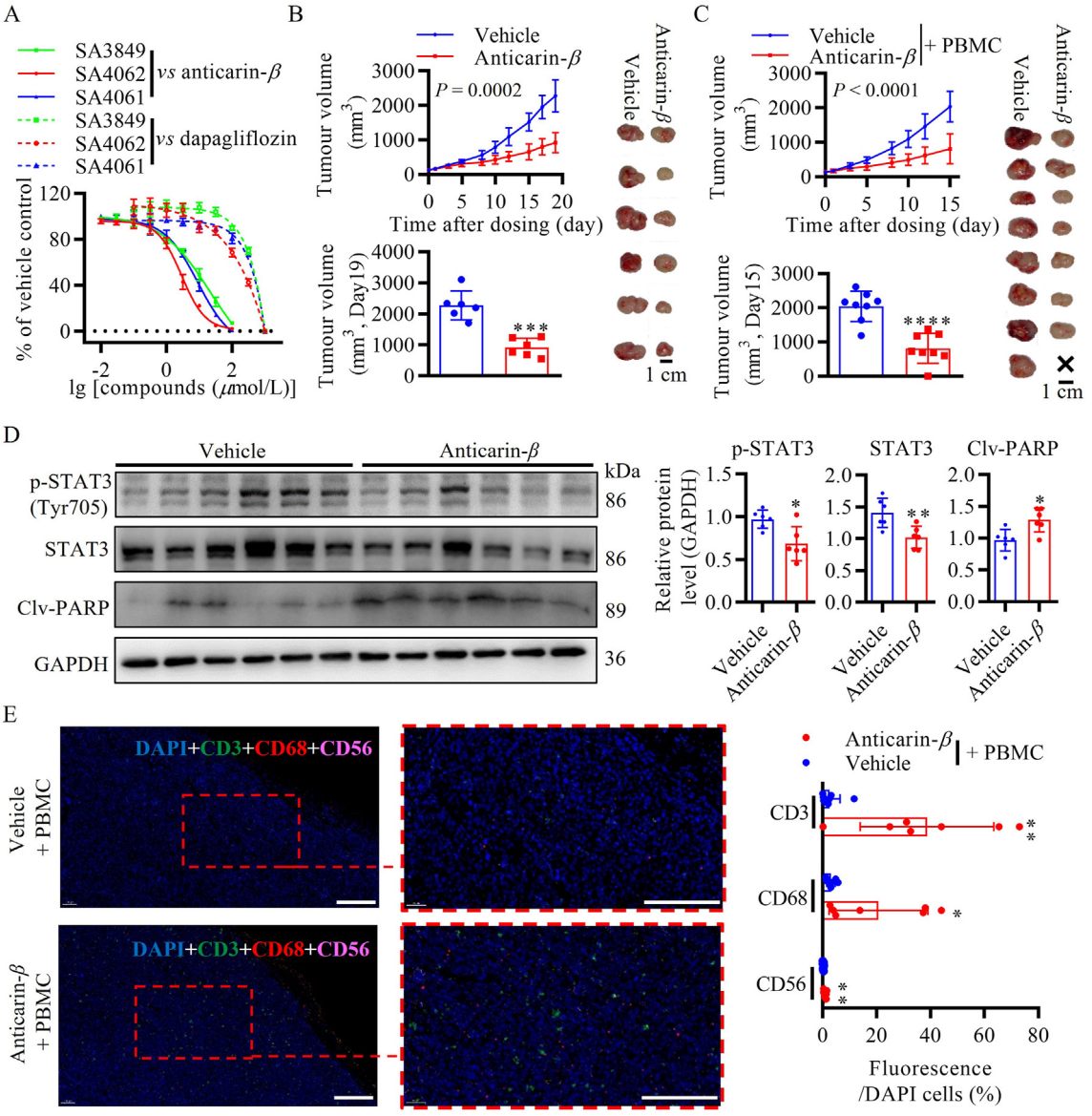

Figure 6 Anticancer effect of anticarin-β in PDX models of OS. (A) *Ex vivo* 3D assay using primary cells isolated from 3 PDX models of OS: SA3849 (post-chemotherapy), SA4061 (post-radiation), and SA4062 (lung metastasis). Dose−response curves of the inhibitory effect by dapagliflozin and anticarin-β are shown. (B, C) Small pieces (approximately 2−3 mm in diameter) PDX model SA4062 tumors were inoculated subcutaneously at the upper right flank region into NOD/SCID ($n = 6$, B) or NCG ($n = 8$, C) mice for tumor development. Groups were randomized when tumor volume reaches 100−150 mm^3 and dosing was initiated at the same time. For peripheral blood mononuclear cell (PMBC) group (C), when mean tumor volume reaches 50−80 mm^3, PBMC were inoculated. Mice were treated daily by intramuscular injection (i.m.) of vehicle control (100 μL) or anticarin-β (5 mg/kg), beginning 23 days after allograft. Graph indicates tumor growth by volume ($W^2 \times L$), assessed three times a week. Inset, image of tumors. Two-way *t*-test analysis of variance. Data represent mean ± SD, scale bars, 1 cm. $^{****}P < 0.0001$, $^{***}P < 0.001$. (D) Tumors from mice treated with anticarin-β or solvent were subjected to Western analysis for cleaved PARP (Clv-PARP), p-STAT3, and STAT3. The intensity of each band was quantified using ImageJ. The data are presented as mean ± SD, $n = 6$; $^{**}P < 0.01$, $^{*}P < 0.05$. (E) Tumors from NCG mice treated with PBMC + anticarin-β or PBMC + solvent were subjected to immunofluorescence analysis for CD3, CD68, and CD56. Anticarin-β significantly increased the infiltration of immune cells into tumor tissue. The data are presented as mean ± SD, $^{*}P < 0.05$, $^{**}P < 0.01$. Scale bar, 200 μm.

SA3849 (post-chemotherapy), SA4061 (post-radiation), and SA4062 (lung metastasis), were used for the *ex vivo* 3D assay. Anticarin-β displayed potent inhibitory effect on all cultures, with the strongest effect on the lung metastasis PDX model SA4062 (Fig. 6A). Next, PDX model SA4062 tumors were subcutaneously inoculated into NOD/SCID mice. As shown in Fig. 6B, compared with vehicle administration, daily administration of 5 mg/kg anticarin-β significantly retarded SA4062 tumor growth (Fig. 6B). More interestingly, anticarin-β combined with peripheral blood mononuclear cell has a better inhibitory effect, these results indicated that anticarin-β could assist immune cells to kill tumor cells (Fig. 6C−E). Consistently, PDX tumors treated with anticarin-β displayed significantly decreased STAT3, p-STAT3 level, and increased cleaved PARP (Fig. 6D). Collectively, these results

demonstrate that anticarin-β markedly impedes tumor growth in different preclinical models of OS without inducing obvious toxicity, indicating that anticarin-β may be effective in treating OS, especially the metastatic/late-stage OS.

4. Discussion

Maintaining proteostasis, including protein synthesis, folding, secretion, and degradation, is critical to the function and viability of cancer cells[29,30]. The chaperonin TRiC is significantly increased in some cancers and strongly correlates with disease progression. The diversification of TRiC subunits into eight paralogs underlies its unique ability to assist the folding of select proteins and function in oncogenesis[19], which prompts us to investigate the functional role of TRiC subunit. Here, our bioinformatic analysis suggests that CCT4/TRiC level tightly correlates with OS progression and prognosis. Consistently, genetic ablation of CCT4 robustly impairs growth and survival of OS cells. The *in vitro* metastatic potential of OS cells is also markedly weakened upon CCT4 inhibition. These findings implicate CCT4/TRiC as a driver of OS progression, and prompt us to search for potential drugs that may specifically inhibit its activity. Encouragingly, after a series of virtual screening and biochemical validation, we identified a natural compound anticarin-β that physically interacts with CCT4. Anticarin-β and CCT4 knockdown lead to the deregulation of numerous common genes and similar pathways in OS cells, advocating that anticarin-β inhibit the activity of CCT4. Anticarin-β displays a selective killing effect in cancer cells, with the highest efficiency in OS cells. Meanwhile, anticarin-β blocks autophagic flux and induces apoptosis in OS cells, again mirroring the effect of genetic inhibition of CCT4. Future structural study should precisely elucidate the amino acid residues and side chains of CCT4 that anticarin-β interacts with.

Interestingly, interrogation of the PRECOG database coincides with the transcriptomic analysis of anticarin-β-treated OS cells, which links anticarin-β efficacy with RTK signaling in OS. Results from a comprehensive array of RTK pathways further reveal that STAT3 signaling is robustly repressed in OS cells upon anticarin-β treatment. Western analysis validates that anticarin-β reduces both phospho- and total forms of STAT3. Since TRiC is recently shown to facilitate STAT3 protein folding and full activation[14], we further verify that anticarin-β impedes the CCT4-mediated maturation of STAT3, leading to the suppressed STAT3 signaling and proteostasis disorder. In keeping with this, the level of CCT4/TRiC and STAT3 is significantly associated in human OS cohorts. Therefore, our results uncover important molecular signaling in OS cells and provide a promising candidate molecule to target it.

Building on the favorable *in vitro* effect and the mechanism of action, we evaluate the *in vivo* efficacy of anticarin-β in preclinical mouse models of OS. Anticarin-β shows stronger antitumor efficacy in an orthotopic model of OS compared to clinical cytotoxic agents, with satisfactory profile of pharmacokinetics and toxicity. Furthermore, of the three PDX tumors modeling different stages of OS, the lung metastasis PDX displays the highest sensitivity to anticarin-β. These results propose anticarin-β as a novel therapeutic agent for OS that worth further preclinical and clinical evaluation.

5. Conclusions

This study unveils an essential role of TRiC−STAT3 signaling in OS progression. Importantly, we demonstrate that inhibiting the CCT4 subunit of the TRiC complex with a natural compound anticarin-β effectively disrupts this signaling network and proteostasis and results in profound antitumor effect in multiple preclinical models of OS. Therefore, our results suggest a promising strategy for the development of CCT4/TRiC-targeted therapeutics for OS treatment.

Availability of data and materials

The original data is available at Mendeley Data (https://data.mendeley.com/datasets/kkgty54cmz/1).

Acknowledgments

We thank Dr. Lian Yang for technical advice and assistance with the ITC analysis. We thank Dr. Lin Zeng for technical advice and assistance with the LC−MS/MS spectrum analysis. We thank Dr. Wenhao Yang for writing advice. This work was supported by funding from the National Natural Science Foundation of China (81903666 and 31930015), the Chinese Academy of Sciences (XDB31000000, KFJ-STS-SCYD-304, and K. C. Wong Education Foundation; China), the Science and Technology Department of Yunnan Province (202101AT070301, 2019ZF003, 202002AA100007, 202003AD150008, and 2019FB103; China), Project of Innovative Research Team of Yunnan Province (2019HC005; China), and the Department of Industry and Information Technology of Yunnan Province (2019-YT-053, China).

Author contributions

Ren Lai, Xia Sheng, Yang Jin, and Gan Wang designed the study and wrote the paper. Gan Wang, Min Zhang, and Ping Meng conducted most of the experiments, analyzed the results, and wrote the paper. Chengbo Long and Yunfei Wang conducted the compound purification experiments. Chengbo Long and Ping Meng conducted the cell-derived xenograft model experiments. Xiaodong Luo, Zhiye Zhang, and Xingwei Yang conducted structural identification experiments. James Mwangi and Peter Muiruri Kamau conducted the RNA experiments. Zunfu Ke, Wenlin Chen, Fei Ge, and Yi Zhang provided clinical samples. Zhi Dai and Xiaodong Luo conducted the qPCR experiments. Dongsheng Li, Qiumin Lv, and Mingqiang Rong provided technical assistance and contributed to the preparation of the figures. All authors analyzed the results and approved the final version of the manuscript.

Conflicts of interest

The authors have declared that no conflict of interest exists.

Appendix A. Supporting information

Supporting data to this article can be found online at https://doi.org/10.1016/j.apsb.2021.12.024.

References

1. Ottaviani G, Jaffe N. The epidemiology of osteosarcoma. *Cancer Treat Res* 2009;**152**:3−13.
2. Moore DD, Luu HH. Osteosarcoma. *Cancer Treat Res* 2014;**162**:65−92.
3. Daw NC, Chou AJ, Jaffe N, Rao BN, Billups CA, Rodriguez-Galindo C, et al. Recurrent osteosarcoma with a single pulmonary

metastasis: a multi-institutional review. *Br J Cancer* 2015;**112**:278−82.
4. Faisham WI, Mat Saad AZ, Alsaigh LN, Nor Azman MZ, Kamarul Imran M, Biswal BM, et al. Prognostic factors and survival rate of osteosarcoma: a single-institution study. *Asia Pac J Clin Oncol* 2017;**13**:e104−10.
5. Isakoff MS, Bielack SS, Meltzer P, Gorlick R. Osteosarcoma: current treatment and a collaborative pathway to success. *J Clin Oncol* 2015;**33**:3029−35.
6. Siegel RL, Miller KD, Jemal A. Cancer statistics, 2018. *CA Cancer J Clin* 2018;**68**:7−30.
7. Han Y, Guo W, Ren T, Huang Y, Wang S, Liu K, et al. Tumor-associated macrophages promote lung metastasis and induce epithelial−mesenchymal transition in osteosarcoma by activating the COX-2/STAT3 axis. *Cancer Lett* 2019;**440**−**441**:116−25.
8. Dai C, Sampson SB. HSF1: guardian of proteostasis in cancer. *Trends Cell Biol* 2016;**26**:17−28.
9. Frydman J, Nimmesgern E, Erdjument-Bromage H, Wall JS, Tempst P, Hartl FU. Function in protein folding of TRiC, a cytosolic ring complex containing TCP-1 and structurally related subunits. *EMBO J* 1992;**11**:4767−78.
10. Joachimiak LA, Walzthoeni T, Liu CW, Aebersold R, Frydman J. The structural basis of substrate recognition by the eukaryotic chaperonin TRiC/CCT. *Cell* 2014;**159**:1042−55.
11. Sternlicht H, Farr GW, Sternlicht ML, Driscoll JK, Willison K, Yaffe MB. The t-complex polypeptide 1 complex is a chaperonin for tubulin and actin *in vivo*. *Proc Natl Acad Sci U S A* 1993;**90**:9422−6.
12. Camasses A, Bogdanova A, Shevchenko A, Zachariae W. The CCT chaperonin promotes activation of the anaphase-promoting complex through the generation of functional Cdc20. *Mol Cell* 2003;**12**:87−100.
13. Cuellar J, Ludlam WG, Tensmeyer NC, Aoba T, Dhavale M, Santiago C, et al. Structural and functional analysis of the role of the chaperonin CCT in mTOR complex assembly. *Nat Commun* 2019;**10**:2865.
14. Kasembeli M, Lau WC, Roh SH, Eckols TK, Frydman J, Chiu W, et al. Modulation of STAT3 folding and function by TRiC/CCT chaperonin. *PLoS Biol* 2014;**12**:e1001844.
15. Vallin J, Grantham J. The role of the molecular chaperone CCT in protein folding and mediation of cytoskeleton-associated processes: implications for cancer cell biology. *Cell Stress Chaperones* 2019;**24**:17−27.
16. Yokota S, Yamamoto Y, Shimizu K, Momoi H, Kamikawa T, Yamaoka Y, et al. Increased expression of cytosolic chaperonin CCT in human hepatocellular and colonic carcinoma. *Cell Stress Chaperones* 2001;**6**:345−50.
17. Yokota S, Yanagi H, Yura T, Kubota H. Cytosolic chaperonin is up-regulated during cell growth. Preferential expression and binding to tubulin at G_1/S transition through early S phase. *J Biol Chem* 1999;**274**:37070−8.
18. Guest ST, Kratche ZR, Bollig-Fischer A, Haddad R, Ethier SP. Two members of the TRiC chaperonin complex, CCT2 and TCP1 are essential for survival of breast cancer cells and are linked to driving oncogenes. *Exp Cell Res* 2015;**332**:223−35.
19. Gestaut D, Roh SH, Ma B, Pintilie G, Joachimiak LA, Leitner A, et al. The chaperonin TRiC/CCT associates with prefoldin through a conserved electrostatic interface essential for cellular proteostasis. *Cell* 2019;**177**:751−765 e15.
20. Jin M, Han W, Liu C, Zang Y, Li J, Wang F, et al. An ensemble of cryo-EM structures of TRiC reveal its conformational landscape and subunit specificity. *Proc Natl Acad Sci U S A* 2019;**116**:19513−22.
21. Reissmann S, Joachimiak LA, Chen B, Meyer AS, Nguyen A, Frydman J. A gradient of ATP affinities generates an asymmetric power stroke driving the chaperonin TRIC/CCT folding cycle. *Cell Rep* 2012;**2**:866−77.
22. Knee KM, Sergeeva OA, King JA. Human TRiC complex purified from HeLa cells contains all eight CCT subunits and is active *in vitro*. *Cell Stress Chaperones* 2013;**18**:137−44.
23. Martinez Molina D, Jafari R, Ignatushchenko M, Seki T, Larsson EA, Dan C, et al. Monitoring drug target engagement in cells and tissues using the cellular thermal shift assay. *Science* 2013;**341**:84−7.
24. Pavel M, Imarisio S, Menzies FM, Jimenez-Sanchez M, Siddiqi FH, Wu X, et al. CCT complex restricts neuropathogenic protein aggregation *via* autophagy. *Nat Commun* 2016;**7**:13821.
25. Kimura S, Noda T, Yoshimori T. Dissection of the autophagosome maturation process by a novel reporter protein, tandem fluorescent-tagged LC3. *Autophagy* 2007;**3**:452−60.
26. Hafner M, Niepel M, Chung M, Sorger PK. Growth rate inhibition metrics correct for confounders in measuring sensitivity to cancer drugs. *Nat Methods* 2016;**13**:521−7.
27. Smirnov P, Kofia V, Maru A, Freeman M, Ho C, El-Hachem N, et al. PharmacoDB: an integrative database for mining *in vitro* anticancer drug screening studies. *Nucleic Acids Res* 2018;**46**:D994−1002.
28. Timofeeva OA, Tarasova NI, Zhang X, Chasovskikh S, Cheema AK, Wang H, et al. STAT3 suppresses transcription of proapoptotic genes in cancer cells with the involvement of its N-terminal domain. *Proc Natl Acad Sci U S A* 2013;**110**:1267−72.
29. Dufey E, Urra H, Hetz C. ER proteostasis addiction in cancer biology: novel concepts. *Semin Cancer Biol* 2015;**33**:40−7.
30. Wang Y, Wang K, Jin Y, Sheng X. Endoplasmic reticulum proteostasis control and gastric cancer. *Cancer Lett* 2019;**449**:263−71.